J Sol-Gel Sci Technol (2018) 85:369–381
DOI 10.1007/s10971-017-4557-y

ORIGINAL PAPER: SOL-GEL AND HYBRID MATERIALS FOR BIOLOGICAL AND HEALTH (MEDICAL) APPLICATIONS

Mesoporous silica SBA-16/hydroxyapatite-based composite for ciprofloxacin delivery to bacterial bone infection

Gracielle Ferreira Andrade[1,2] · Jerusa Araújo Quintão Arantes Faria[3] · Dawidson Assis Gomes[4] · André Luís Branco de Barros[2] · Renata Salgado Fernandes[2] · Amanda Cristina Soares Coelho[5] · Jacqueline Aparecida Takahashi[5] · Armando da Silva Cunha Jr[2] · Edésia Martins Barros de Sousa[1]

Received: 6 July 2017 / Accepted: 27 November 2017 / Published online: 20 December 2017
© Springer Science+Business Media, LLC, part of Springer Nature 2017

Abstract The development of systems that can prevent infections and also ensure bone integration as well as regeneration have been of great interest for pharmaceutical technology. In this study, we show the synthesis of surface-functionalized mesoporous silica (SBA-16) and silica composed of calcium phosphate (SBA-16/HA) particles in order to be applied as efficient drug delivery carriers. The particles were synthesized, functionalized with 3-aminopropyltriethoxysilane (APTES) by post-synthesis grafting and loaded with the osteomyelitis antibiotic agent ciprofloxacin. Moreover, the diethylenetriaminepentacetic acid (DTPA) was anchored in silica-APTES to allow measurements of biological process at molecular and cellular levels. Particles were physicochemically characterized by small angle X-ray scattering (SAXS), elemental analysis (CHN), thermogravimetric analysis (TGA), N_2 adsorption and zeta potential analysis. Functionalized silica particles were radiolabeled with technetium-99m showing high radiochemical yields and high radiolabeled stability. In vivo experiments results showed higher bone uptake of the SBA-16/HAAPTES than SBA-16APTES. In addition, bactericidal efficacy of these particles was tested against microorganisms present in bone infection, and our composites had bactericidal efficiency comparable to free-ciprofloxacin. In summary, taking into account the great potential of these silica mesoporous and nanocomposite structures to carry molecules, besides their bactericidal efficacy, these materials are promising candidates for bone infection treatment.

Graphical abstract

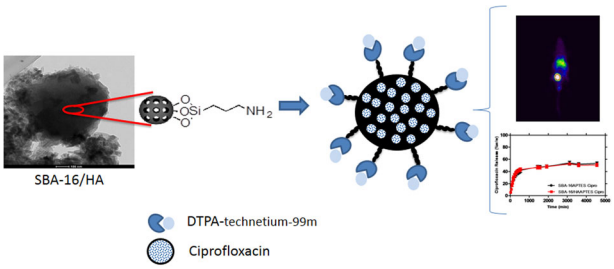

The ciprofloxacin loading studies in particles, drug release efficiency and *in vivo* preferential uptake bone of the composite were observed.

Keywords Mesoporous silica/hydroxyapatite composite · 3-aminopropyltriethoxysilane-APTES · Ciprofloxacin · Bactericidal activity · Technetium-99m

✉ Edésia Martins Barros de Sousa
sousaem@cdtn.br

[1] Center of Development of the Nuclear Technology, CDTN/CNEN, Belo Horizonte, Brazil

[2] Faculty of Pharmacy, Federal University of Minas Gerais—UFMG, Belo Horizonte, Brazil

[3] Institute of Biological Science—Departament of Physiological Sciences, Federal University of Amazonas—UFAM, Manaus, Brazil

[4] Institute of Biological Science—Departament of Biochemistry and Immunology, Federal University of Minas Gerais—UFMG, Belo Horizonte, Brazil

[5] Institute of Exact Sciences—Departament of Chemistry, Federal University of Minas Gerais—UFMG, Belo Horizonte, Brazil

1 Introduction

The impact of bone diseases and trauma has increased significantly in the last decades around the world. The prevalence of aging-related diseases due to the increase in life expectancy and obese population has led to an increase in demand for bone repair and bioactive materials with application in therapies for bone disorders [1].

Bone diseases, like osteomyelitis, which are caused by microorganisms, are highly complicated and involve operative debridement and removal of all foreign bodies followed by antimicrobial therapy. As antimicrobial treatments often involve a long course of therapy, sufficient antibiotic exposure is needed to ensure the eradication of the microorganisms [2]. However, intensive and inappropriate use of antibiotics can select resistant microorganisms and has dramatically increased the frequency of resistance among human pathogens promoting favorable conditions for infections to emerge, spread and persist [3, 4].

Among the microorganisms involved in bone infections the most important pathogens are *Staphylococcus aureus* and *Pseudomonas aeruginosa*, Gram-positive and Gram-negative bacteria, respectively [2]. Fluoroquinolones are potent antibacterial agents which target two related enzymes, DNA gyrase and DNA topoisomerase IV [5]. Ciprofloxacin, a broad-spectrum fluoroquinolone antibacterial agent is potent against a wide range of Gram-positive and Gram-negative pathogenic bacteria [6].

The concentration of antibiotics administrated by systemic route is low in bone tissue due to the limited blood circulation in these infected sites [7]. Thus, effective drug concentration is not achieved at the site of infection [2]. It is recognized that extended-release preparation is advantageous to improve patient compliance, as the frequency of administration can be reduced by maintaining a constant plasma drug concentration over a prolonged period of time [8]. Because of that, we sought to obtain a high local dose at the specific infected bone site from ciprofloxacin-loaded inorganic bone composite such as silica/hydroxyapatite.

A facile sol–gel synthetic method to produce silica with mesoporous structure provides an extremely attractive matrix for integrating other chemical compounds such as hydroxyapatite to form nanocomposites, which have been widely used as bone-tissue regeneration systems [9]. Inorganic bone matrix is composed of carbonated hydroxyapatite. Accordingly, the vast majority bioactive materials are based on ceramics and glasses containing silicate ions and calcium phosphates [10, 11]. Moreover, drug delivery systems based on these nanocomposites have also been developed to enhance bone ingrowth and regeneration during treatment of bone defects [12, 13], besides presenting characteristics such as excellent biocompatibility, bioactivity, low susceptibility to immune response, and resistance to lipases and bile salts [14]. Furthermore, inorganic particles can not only improve the resistance of therapeutic agents against enzymatic degradation but also provide the possibility of transporting biomolecules to specific tissues, cells and cell compartment in a controlled manner [14].

In a previous work, a mesoporous silica particle/hydroxyapatite (SBA-16/HA) hybrid drug carrier was produced by homogeneously incorporating calcium and phosphate salt into silica particles. SBA-16 and SBA-16/HA were previously investigated for their structural and physicochemical characteristics. Moreover, in vitro assays indicated that the as-synthesized SBA-16/HA nanocomposites can be used as an attractive and promising drug delivery system for application in bone therapy [15, 16].

In this work, these particles were surface-modified with APTES, which improves the drug-loading, drug release efficiency, and enables the anchoring of DTPA for chelating of technetium-99m, revealing the increased uptake of SBA-16/HA nanocomposite compared to the SBA-16 in the bone region. The ciprofloxacin loading and release was elucidated to optimize antibiotic release for local treatment of osteomyelitis. Therefore, in this paper the in vitro cytotoxicity, drug release behavior, antibacterial activity and in vivo preferential uptake bone effect of the hybrid materials functionalized with APTES and DTPA were investigated.

2 Materials and methods

2.1 Materials

Tetraethyl-orthosilicate (TEOS), 3-amino-propyltriethoxysilane (APTES), Phosphate Buffer Saline (PBS), Fetal Bovine Serum (FBS), Penicillin–Streptomycin 50 lM, 3-(4,5-dimethiol-2-thioazolyl)-2,5-diphenyl tetrazolium bromide (MTT), CellTiter-Blue®, Pluronic F-127 (Mav = 12,600), solvents (HPLC analytical grade) and diethylenetriaminepentaacetic dianhydride were purchased from Sigma-Aldrich (São Paulo, Brazil). Dulbecco's modified Eagle's medium (DMEM) was purchased from Invitrogen (São Paulo, Brazil). Technetium-99m was obtained from an alumina-based $^{99}Mo/^{99m}Tc$ generator.

2.2 Synthesis of mesoporous silica SBA-16

Silica-block copolymer mesophases were synthesized using Pluronic F127 (poly(ethylene oxide)-block-poly(propylene oxide)-block-poly(ethylene oxide)), $M_{av} = 12{,}600$, as a templating agent at room temperature. 3.0 g of Pluronic F127 was dissolved in 144 mL of water and 13.9 mL of 38% hydrochloric acid (HCl) solution under constant stirring at 25 °C. After approximately 30 min, 11 mL of co-surfactant butanol was added to reach a 1:3 (F127:BuOH) mass ratio in the ternary system. Next, 15.3 mL of tetraethyl orthosilicate (TEOS, Sigma-Aldrich, São Paulo, Brazil) was added to the solution under constant stirring at 45 °C for 1 h, according to the method reported by Gobin [17] with

modifications. After aging at 100 °C for 24 h in a hermetically closed recipient, the solids were collected by filtration and dried in open air at 37 °C. The surfactant was removed by calcination, which was carried out by increasing the temperature to 550 °C under nitrogen flow for 5 h. Chemical analysis showed that the surfactant had been completely removed by this thermal treatment.

2.3 Synthesis of SBA-16/HA composite

The synthesis of the material was carried out using a two-step procedure, which is detailed in the following two sections.

2.3.1 Preparation of the calcium-doped silica matrix

The first step (low pH step) consisted on the preparation of a calcium doped silica matrix which was obtained by means of a variation of the methodology described by Dìaz et al. [18]. Silica-block copolymer mesophase SBA-16/HA composites were synthesized using Pluronic F127 (poly (ethylene-oxide)-block-poly(propylene-oxide)block-poly (ethylene-oxide)), $M_{av} = 12{,}600$, as a structure reacting agent, which was reacted at room temperature. In a typical preparation, 3.0 g of Pluronic F127 was dissolved in 200 mL of $Ca(NO_3)_2$ solution and 100 mL of HCl 2 M solution with constant stirring at 25 °C. After approximately 30 min, 11 mL of the co-surfactant butanol was added to reach a 1:3 (F127: BuOH) mass ratio in the ternary system. Next, 15.3 mL of TEOS (Sigma-Aldrich) were added to the solution, under vigorous stirring at 45 °C for 1 h, according to the method reported by Gobin [17], and then aged at 100 °C for 24 h in a hermetically closed recipient. Then, the product was dried in an oven at 100 °C.

2.3.2 HA crystallization in the Ca-doped matrix

In the second step (high pH step), the Ca-doped silica was dropped into a $(NH_4)_2HPO_4$ solution, and the pH value was adjusted to 9. Then, the solution was subjected to a second hydrothermal treatment at 100 °C for 24 h. The powder was then washed and heat-treated in open air at 600 °C for 6 h to obtain the final (HA/SBA-16) material [18].

2.4 Functionalization of SBA-16 and SBA-16/HA composite

2.4.1 Functionalization with APTES

The functionalization process has been performed through reaction between silica mesoporous material and 3-aminopropyltriethoxysilane—APTES, under reflux in toluene, according method described previously [19, 20]. The obtained materials were denominated SBA-16APTES and SBA-16/HAAPTES.

2.4.2 Functionalization of SBA-16APTES and SBA-16/HAAPTES with DTPA

SBA-16APTES and SBA-16/HAAPTES (20 mg in 1 mL of citrate buffer, pH 8) were reacted with 0.06 mmol of diethylenetriaminepentaacetic dianhydride in DMSO (100 µL). The solutions were stirred at room temperature overnight. The DTPA-SBA-16APTES and DTPA-SBA-16/HAAPTES solutions were purified by centrifugation (5000 *x g* for 5 min). The pellet was ressuspended with 1 mL of citrate buffer and centrifuged again, this procedure was repeated three times [21].

2.5 Physicochemical and morphological characterization of SBA-16, SBA-16APTES, SBA-16/HA and SBA-16/HAAPTES composites

All the samples were physicochemically characterized by small angle X-ray scattering (SAXS), elemental analysis (CHN), thermogravimetric (TGA), N_2 adsorption/desorption and zeta potential analysis. The small-angle X-ray diffraction patterns were obtained using synchrotron radiation. The incident X-ray was set at a wavelength of 1.488 Å, and the scattering angle ranged from 0° to 5°. Synchrotron radiation measurements were carried out at the D2A beamline of the Brazilian Synchrotron Light Laboratory (LNLS, Campinas, Brazil). Aiming to evaluate the functionalization process in silica particles, the number of hydrocarbon chains in the material pore wall was analyzed by TGA and elemental analysis. TGA measurements were taken in a Shimadzu TGA 50WS with temperature ranging from 25 to 800 °C. Approximately 5.0 mg of the starting mixture and the final sample were analyzed using a heating rate of 10 °C min^{-1}, in nitrogen (N_2) atmosphere, flow rate of 50 mL min^{-1}, in an open alumina crucible. Elemental analysis was performed in a Perkin–Elmer CHNSO model 2400. Nitrogen adsorption isotherms of samples were obtained at 77 K using a Quantachrome SiQwin™- Automated Gas Sorption Data adsorption analyzer. Before the adsorption measurements, SBA-16, SBA-16APTES, SBA-16/HA and SBA-16/HAAPTES were outgassed for 48 h at 40 °C before analysis. All data analyses were performed using the NovaWin, 1994–2011 Quantachrome Instruments software (Boynton Beach, FL, USA). The analytical procedure to perform zeta potential analysis was conducted in a Zetasizer Nanoseries Zs (Malvern Instruments, Malvern, UK) apparatus after the adequate dilution of the samples in ultra-pure MilliQ water (pH 7.0).

2.6 Drug loading and in vitro release study

The adsorption of ciprofloxacin within SBA-16APTES and SBA-16/HAAPTES composites was performed by soaking 100 mg of the powder sample in a drug solution (1000 µg/mL) and kept under magnetic stirring for 48 h. The ciprofloxacin solution was subjected to pH variation to obtain complete solubilization of the drug. Initially, the pH of the solution was reduced to pH 2, using HCl 2 M; subsequently, the pH was raised to ~ 4 using sodium hydroxide (NaOH) 1 M. The mixture was filtered, washed with distilled water and dried for 24 h at 60 °C. Elemental analysis and TGA measurements were performed in all samples to evaluate the percentage of ciprofloxacin adsorbed. In addition to the CHN and TGA measurements, UV-VIS spectroscopy was used to assess the drug content remaining in the supernatant by measuring the concentration of ciprofloxacin before and after the loading procedure. For release assays, SBA-16APTES and SBA-16/HAAPTES samples were immersed in simulated body fluid (SBF) (1.5 mL, pH ~7.3). This suspension was put into a dialysis tube (cutoff Mn = 3500) and then placed in a flask with 38.5 mL of SBF under constant stirring at 50 rpm [22]. The UV spectrometry procedure (Shimadzu UV-VIS V-2401) was used to monitor the amount of loaded and released ciprofloxacin as a function of time. The concentration of ciprofloxacin in SBF was determined by the intensity of the absorption band at 275 nm. The in vitro experiments were carried out in triplicate.

2.7 Cell culture

Human embryonic kidney cell line HEK 293 was obtained from American Type Culture Collection (ATCC Number: CRL-1573; ATTT). Cells were maintained at 37 °C in 5% CO_2 in DMEM (Sigma-Aldrich) containing 10% fetal bovine serum, 5 mM sodium pyruvate, 100 U/mL penicillin, 0.1 mg mL^{-1} streptomycin and 0.25 mg mL^{-1} Amphotericin B (Life Technologies). Cells were grown in T75 Flasks to 70% confluence before routine weekly passage by trypsinization.

2.8 Cytotoxicity studies

The MTT and CellTiter assays were employed to determine the cytotoxicity of pure, functionalized and ciprofloxacin-loaded silica particles (SBA-16, SBA-16APTES, SBA-16APTES Cipro, SBA-16/HA, SBA-16/HAAPTES and SBA-16/HAAPTES Cipro), sterilized under UV light. Confluent HEK 293 cells in the fourth passage were used in both experiments. 1.0×10^4 cells/well were seeded on 96 well flat plates for 24 h in an incubator with an atmosphere of 5% CO_2 at 37 °C. For MTT assay, cells were treated with samples concentrations ranging from 1.25 to 1000.0 µg mL^{-1}, and the results are expressed in function of the log dose. After 48 h of incubation at 37 °C, MTT was added to each well. After 4 h of incubation, SDS 10% HCl was added to each well to dissolve formazan crystals and the plate was incubated for 18 h at 37 °C. The absorbance was measured at 595 nm using a microplate reader (ELX 800 BIOTEK Instruments Inc).

To confirm the results obtained from MTT assay, cell viability was also evaluated by CellTiter-Blue® assay, an optimized reagent containing resazurin. After the sample treatment, the CellTiter reagent was added directly to the cells at the ratio of 20 to100 µL of reagent:culture medium. The plates were incubated at 37 °C for 4 h to allow viable cells to convert resazurin to the fluorescent resorufin product, and recorded at $560_{Ex}/590_{Em}$. The conversion of resazurin to fluorescent resorufin is proportional to the number of metabolically active, viable cells, present in this population. Cell viability or cell metabolism was expressed as a percentage relative to the untreated cells (control). The experiments were carried out in triplicate.

2.9 Antimicrobial screening

The antimicrobial activity of the particles was investigated against *Staphylococcus aureus*, *Pseudomonas aeruginosa*, *Escherichia coli* and *Bacillus cereus*. A stock aqueous solution was prepared from the different inorganic samples (12.5 mg mL^{-1}). A pre-inoculum was prepared in which the bacteria stored in test tubes were transferred with platinum loop and inoculated into test tubes containing 3.0 mL of Brain Heart Infusion (BHI) culture medium. Then, the tubes were incubated in an oven at 37 °C for 24 h. 500 µL of the pre-inoculum bacterial suspension were transferred to flasks containing sterile distilled water. The suspension concentration was adjusted to 600 nm until a transmittance between 74% and 75% following 0.5 McFarland turbidity standards is achieved. The test solution was prepared by pipetting 40 µL of the stock solution into 960 µL of BHI culture medium.

The experiments were performed with 100 µL of the test solution distributed in 96–well plates and 100 µL of the bacterial inoculum. Four control groups were conducted; one for growth control of the microorganism (to assure cell viability), the blank, without bacterial inoculum, a quality control of the assay (the working solution replaced by an antibiotic) and a sterility control of the medium containing 100 µL of BHI culture medium and 100 µL of sterile distilled water. The microplates were incubated at 37 °C, during 24 h. The experiments were performed in quintuplicate and the absorbances were determined using an ELISA tray reader (Thermoplate, Brazil) at a fixed wavelength of 490 nm. The final concentration tested in the test

was 250 μg mL^{-1}. The control antibiotic used was ampicillin [23].

2.10 Radiolabeling

The samples were radiolabeled according to the following procedure: 1 mg of DTPA-SBA-16APTES or DTPA-SBA-16/HAAPTES, 80 μL of 4.5 mM $SnCl_2{\cdot}2H_2O$ solution in 0.1 M HCl and 0.5 mL of 0.9% NaCl (w/v) were added to a sealed vial. The pH was adjusted to 7 with 30 μL of NaOH (1 mol L^{-1}). Then, an aliquot of 0.5 mL of $Na^{99m}TcO_4$ (37 MBq) was added. The solution was allowed to react for 15 min at room temperature under stirring. Afterwards, the vial was centrifuged (10,000x*g*, 5 min). The nanoparticles were suspended with 1 mL of 0.9% NaCl (w/v), reaching a final nanoparticle concentration of 1 mg mL^{-1}.

2.10.1 Radiochemical yield

Radiochemical yield analyses were performed by thin layer chromatography on silica gel (TLC-SG, Merck). TLC-SG analysis was accomplished using methylethylketone, as mobile phase, to determine the amount of free technetium-99m. $^{99m}TcO_2$ and $^{99m}TcO_4^-$ were removed from the preparation during the centrifugation step, since they remained in the supernatant after the centrifugation. The radiochemical yield (%R) was calculated by Eq. (1)

$$\%R = (\text{radioactivity in the pellet}/\text{total radioactivity in the flask}) \times 100 \quad (1)$$

2.10.2 In vitro stability

In vitro studies were performed for ^{99m}Tc-DTPA-SBA-16APTES and ^{99m}Tc-DTPA-SBA-16/HAAPTES. The stability was tested in the presence of 0.9% NaCl (w/v) solution and mice plasma. The NaCl 0.9% (w/v) stability was evaluated at room temperature and plasma stability was carried out at 37 °C under agitation. Aliquots were taken out at 1, 2, 4, 6, and 24 h, and analyzed by TLC, as previously described.

2.10.3 Biodistribution studies

Aliquots of 3.7 MBq of the ^{99m}Tc-DTPA-SBA-16APTES or ^{99m}Tc-DTPA-SBA-16/HAAPTES were injected intravenously into healthy Swiss mice ($n = 6$). After 1 and 4 h, mice were anesthetized with a mixture of xylazine (15 mg kg^{-1}) and ketamine (80 mg kg^{-1}). Whole liver, spleen, kidney, stomach, heart, lungs, blood, muscle, and thyroid were all removed, dried on filter paper, and placed in preweighed plastic test tubes. The radioactivity was measured using an automatic scintillation apparatus. A standard dosage containing the same injected amount was counted simultaneously in a separate tube, which was defined as 100% radioactivity. The results were expressed as the percentage of injected dose/g of tissue (%ID/g). All animal studies were approved by the local Ethics Committee for Animal Experiments of Federal University of Minas Gerais —Brazil (protocol number: 343/2014).

2.11 Statistical analysis

Significance of changes in treatment groups was determined by ANOVA and Bonferroni's multiple comparison tests using Prism 6 software. Data are represented as the mean ± standard error of the mean (SEM).

3 Results and discussion

3.1 N_2 adsorption/desorption

An assessment of the pore structure of the all functionalized and ciprofloxacin loaded samples was performed using N_2 adsorption/desorption isotherms and the results are shown in Fig. 1. Data of SBA-16 and SBA-16/HA materials were used for comparison [16]. All samples exhibit a type IV isotherm, characteristic of mesoporous materials. HA/SBA-16 shows a H3-type hysteresis loop, which is often observed with aggregates of plate-like particles, which in turn give rise to slit-shaped pores [18]. As can be observed in Table 1, this result reveals a decrease in pore volume and shows that the presence of HA in the SBA-16 matrix leads to a significant decrease in the surface area, as described by ANDRADE et al. [16]. As expected, the introduction of the organic moieties, APTES, leads to a decrease in surface area and in the pore volume (Table 1). This decrease evinces the

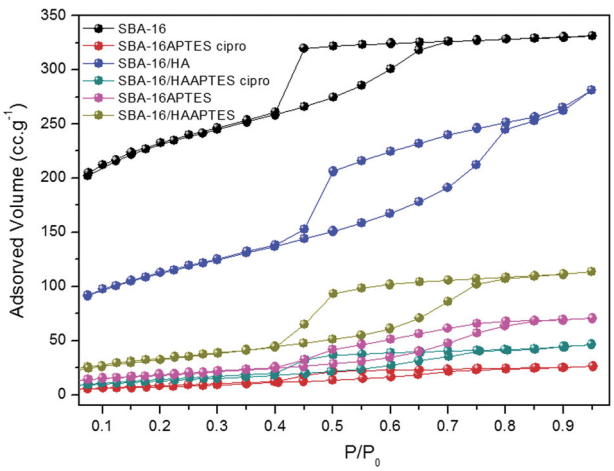

Fig. 1 Nitrogen adsorption–desorption isotherms

Table 1 N_2 adsorption/desorption parameters of SBA-16, SBA-16APTES, SBA-16APTES Cipro, SBA-16/HA, SBA-16/HAAPTES, and SBA-16/HAAPTES Cipro samples

Samples	D_p (nm)	S_{BET} ($m^2\ g^{-1}$)	V_p ($cc^3\ g^{-1}$)
SBA-16	3.4	735	0.244
SBA-16APTES	3.4	98	0.117
SBA-16APTES Cipro	3.4	29	0.040
HA/SBA-16	3.8	384	0.351
SBA-16/HAAPTES	3.8	122	0.204
SBA-16/HAAPTES Cipro	3.8	49	0.070

N_2 adsorption error: 3%

S_{BET} the specific area, D_p the average pore diameter, V_p the average pore volume

fact that organic material is located within the pores of the matrices. The same behavior was also observed for the drug loaded samples. The pore size distribution curves (not shown) for pure and modified samples show a very narrow pore size distribution of the mesopores at around 3.4 nm for SBA-16 and 3.8 nm for SBA-16/HA, calculated by using the BJH computation procedure.

3.2 Small-angle X-ray scattering (SAXS)

SAXS patterns of as-made materials confirm that they are highly ordered, as demonstrated in a previous paper [15]. Figure 2 shows the SAXS patterns of SBA-16 and SBA-16/HA samples, which revealed one intense peak related to the (110) diffraction plane, and two lesser peaks related to the (200) and (211) planes. The SAXS patterns of functionalized silica SBA-16 and SBA-16/HA are presented in insert. The type of mesostructure can be identified by analyzing the relative peak distance ratios ($q_{1\ 1\ 0}/q_{1\ 1\ 0}$, $q_{2\ 0\ 0}/q_{1\ 1\ 0}$ and $q_{2\ 1\ 1}/q_{1\ 1\ 0}$). The three peaks, whose positions are in a $q_{h\ k\ l}/q_{1\ 1\ 0}$ ratio of 1:√2:√4:√6 (h, k and l are the Miller Indices), correspond, respectively, to the (1 1 0), (2 0 0) and (2 1 1) diffraction planes of the cubic (Im3m) mesophases formed by the compact packing of cylindrical tubes [24]. It is noteworthy that functionalized samples also exhibit a well-resolved peak indexed as (110), typical of ordered cubic mesoporous structures (insert Fig. 2). Indeed, the intense peak related to the (110) SAXS reflection remained present after hydrocarbon chain incorporation in SBA-16APTES and SBA-16/HAAPTES samples, suggesting only a small loss of structural ordering in the host mesostructure [25].

In addition to the characteristic reflections, the position of the first peak at around 2θ of 0.74 for SBA-16 and 0.72 for SBA-16/HA allows direct determination of the center–center distance between adjacent tubes using $a_0 = d_{(110)}\cdot\sqrt{2}$ and $d = \lambda/\sin\ 2\theta$, where d corresponds to the interplanar distances, and a_0 is the unit cell parameter [24]. Table 2 summarizes these results. In the case of SBA-16, its characteristic cubic structure had a corresponding unit cell parameter of $a_0 = 16.3$ nm with d_{110} spacing of 11.5 nm. The value of a_0 was calculated at 16.7 nm with d_{110} spacing of 11.8 nm for SBA-16/HA. The SAXS patterns of surface modified SBA-16APTES and SBA-16/HAAPTES samples showed a_0 values of 16.3 and 16.9 nm and $d_{(110)}$ values of 11.5 and 12.0 nm, respectively. These results indicated that pore wall functionalization does not affect the structural order. Nevertheless, nanocomposites samples present broader diffraction peaks, indicating that the structure of these materials are less regular than SBA-16. It is not surprising that the pattern for SBA-16 is sharper than that for nanocomposites, given that the former exhibited much more uniform mesopores, as shown by the adsorption isotherms in Fig. 1. Calculated d_{110}, a_0 and h (pore wall thickness) values are reported in Table 2. Pore wall thicknesses (h) were evaluated from geometrical considerations and unit-cell parameters ($h = a - D_p$), where D_p is pore size obtained from N_2 adsorption. As expected, an increase in mesopore diameter was observed for nanocomposite samples, as previously described by Dìaz [18]. The increase in the average pore size diameter can be due to the growth of HA crystals, which can block the available space of the mesoporous silica. As discussed in a previous work [15], the pores within the mesopore range can act as initiation sites for HA crystal nucleation, suggesting that increasing levels of calcium and phosphate ions inside the pores promoted the precipitation of HA within this region.

3.3 Thermogravimetry analysis (TGA) and elemental analysis (CHN)

The TGA curves of all the systems are shown in Fig. 3 and the results are summarized on Table 3. For comparison, data from a previous work is shown [16], the SBA-16 and SBA-16/HA samples show initial weight losses of 16.8 and 7.8%, respectively, from 25 to 150 °C, which is apparently due to the thermodesorption of physically adsorbed water. Above 150 and up to 800 °C, no significant weight loss could be identified. The SBA-16 and HA/SBA-16 materials have adequate thermal stability for application where this characteristic is desirable. It was possible to see small weight losses during temperature variation of the pure matrices.

The amount of functionalized agent anchored in the matrices SBA-16APTES and SBA-16/HAAPTES as well as the amount of ciprofloxacin incorporated inside of these matrices were estimated by TGA technique (Table 3).

In the cases of functionalized samples, weight loss occurred in two distinct regions for all samples. The first region of weight loss occurs in a temperature range between 25 and 150 °C, which can be attributed to thermodesorption of physically adsorbed water. The second region showed

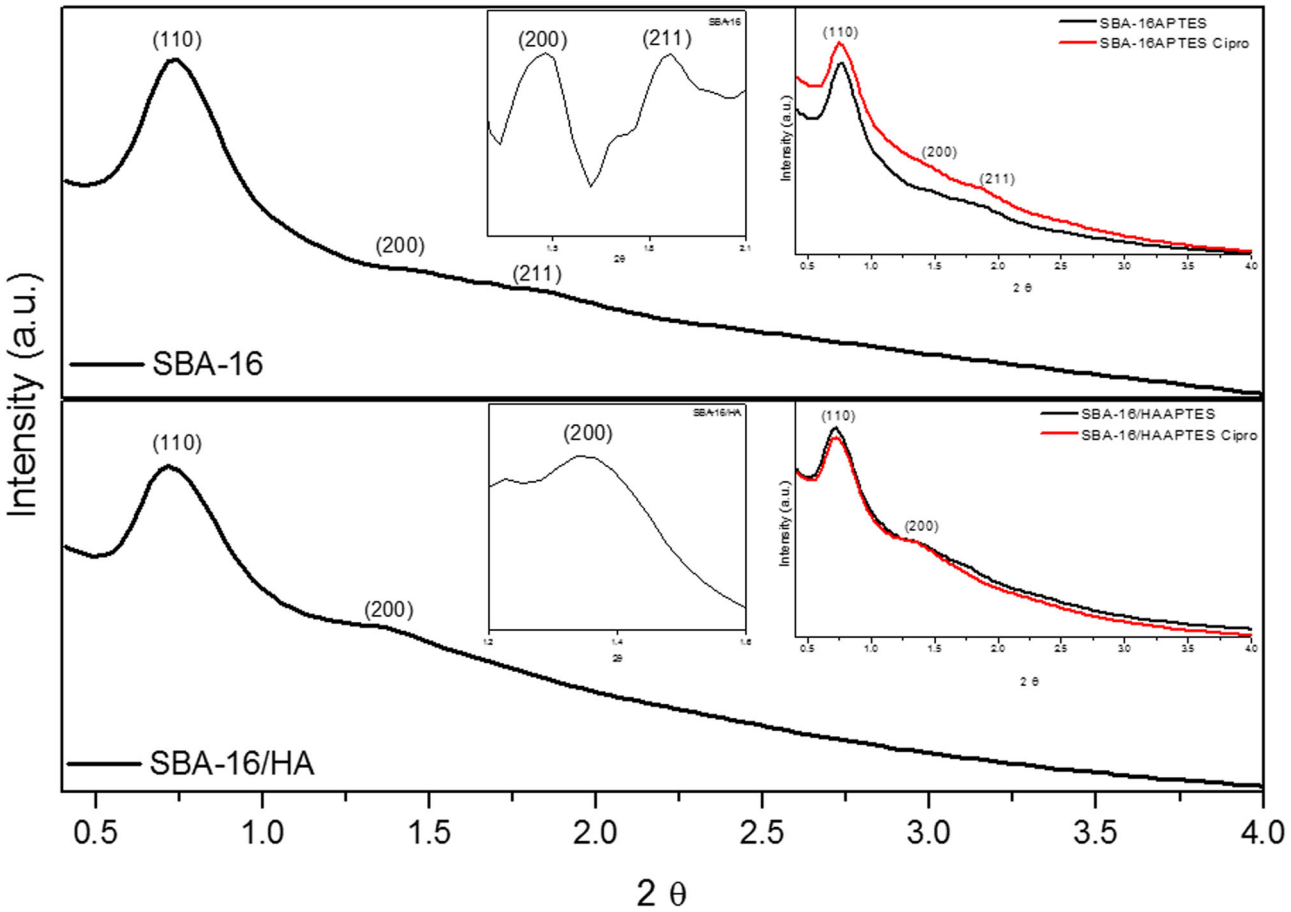

Fig. 2 SAXS patterns of SBA-16, SBA-16APTES, SBA-16APTES Cipro, SBA-16/HA, SBA-16/HAAPTES, and SBA-16/HAAPTES Cipro samples

Table 2 Structural parameters of SBA-16, SBA-16APTES, SBA-16/APTES Cipro, SBA-16/HA, SBA-16/HAAPTES, and SBA-16/HAAPTES Cipro samples

Samples	2 θ	d_{110} (nm)	a_0 (nm)	h (nm)
SBA-16	0.74	11.5	16.3	12.9
SBA-16APTES	0.74	11.5	16.3	12.9
SBA-16APTES Cipro	0.74	11.5	16.3	12.9
SBA-16/HA	0.72	11.8	16.7	12.9
SBA-16/HAAPTES	0.71	12.0	16.9	13.1
SBA-16/HAAPTES Cipro	0.71	12.0	16.9	13.1

weight loss between 150 and 600 °C, which can be attributed to the decomposition temperature for incorporated alcoxysilane groups. The presence of the hydrocarbon chain, as observed in APTES molecules, gives the wall surface a rather hydrophobic characteristic. As a consequence, the mass loss due to water molecules in the pore interface, in the first region (25–150 °C), is much lower for the APTES when compared to non-functionalized silica-SBA16 samples. The TGA was also used to infer the amount of ciprofloxacin loaded in each sample and the data

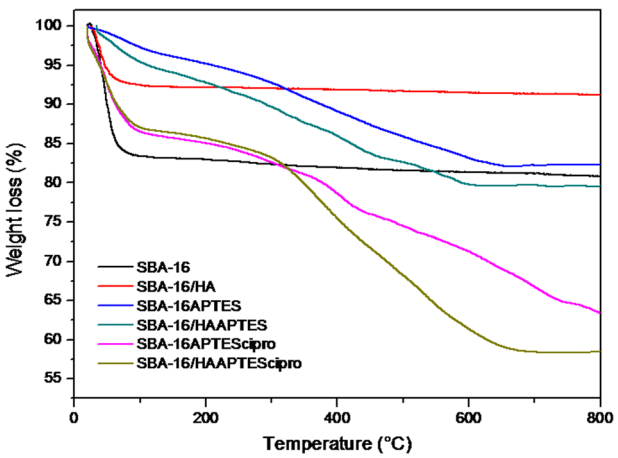

Fig. 3 TG curves for SBA-16, SBA-16APTES, SBA-16APTES Cipro, SBA-16/HA, SBA-16/HAAPTES, and SBA-16/HAAPTES Cipro samples

found confirms the presence of the drug in the pores after the adsorption of the drug. It is worth to mention that the results show that ciprofloxacin adsorbed in the SBA-16APTES matrix remains practically the same respective to

Table 3 Percentage of weight loss and elemental analysis of SBA-16, SBA-16APTES, SBA-16APTES Cipro, SBA-16/HA, SBA-16/HAAPTES, and SBA-16/HAAPTES Cipro samples

Samples	Weight loss (% w/w) 25–150 °C	Weight loss (% w/w) 150–800 °C	Residue (% w/w) > 800 °C	C (%)	N (%)
SBA-16	16.8	2.3	80	0.2 ± 0.01	0.02 ± 0.01
SBA-16APTES	3.9	13.9	82	6.9 ± 0.1	2.61 ± 0.01
SBA-16APTES Cipro	14.3	22.3	63	15.9 ± 0.9	3.9 ± 0.1
SBA-16/HA	7.8	1.0	91	0.17 ± 0.01	0.03 ± 0.01
SBA-16/HAAPTES	5.9	14.4	79	6.1 ± 0.2	1.81 ± 0.04
SBA-16/HAAPTES Cipro	13.6	27.9	58	15.5 ± 0.2	3.4 ± 0.05

the HA/SBA-16APTES, as no statistically significant differences could be observed in the loading percentage. Considering that the pore sizes of the SBA-16APTES and HA/SBA-16APTES are large enough to entrap ciprofloxacin, it can be concluded that the similar degree of functionalization of these samples contributes to the comparable capacity of drug loading in both the matrices.

Evidence that surface modification with APTES and incorporation of ciprofloxacin occurred in the SBA-16 and HA/SBA-16 matrices was also obtained through elemental analysis. This technique indicates an increase in the percentages of the carbon (C) and nitrogen (N) elements in SBA-16 and HA/SBA-16, where APTES functionalization and drug loading occurred. Table 3 shows the value contents of this element in the matrices after APTES anchoring and drug loading. The results indicate that the APTES group and ciprofloxacin drug were incorporated in the structure of SBA-16 and HA/SBA-16. As previously mentioned in the TGA analysis, the high percentage of carbon and nitrogen produced by the incorporation suggested a relatively high level of drug loading. By comparing the drug incorporation of the two samples (SBA-16APTES and HA/SBA-16APTES), no differences were observed in C content (%) and N content (%), confirming the results obtained from TGA.

3.4 Zeta potential analysis

Zeta potential measurements are used to characterize the surface charges of particles. Table 4 shows the values of zeta potential measurements for SBA-16, SBA-16APTES, SBA-16/HA, and SBA-16/HAAPTES. The mean zeta potential value of free SBA-16 and SBA-16/HA are −56.0 ± 2.3 and 2.9 ± 1.9 mV, respectively. This result of SBA-16 is due to the high amount of silanol groups on the silica surface [26]. However, for SBA-16APTES and SBA-16/HAAPTES particles, the values are 25.2 ± 5.0 and 30.4 ± 1.3 mV, respectively. Changes could be attributed to incorporation of amino groups onto the silica surface. The results indicate the successful modification of the outer surface of the matrices by APTES. The same reduction happened after binding with DTPA due to carboxylic acid present in the molecule. Nevertheless, SBA-16/HAAPTES DTPA samples showed positive charge.

Table 4 Zeta potencial analysis

Samples	ζ potential ± SD (mV)
SBA-16	−56.0 ± 2.3
SBA-16APTES	+25.2 ± 5.0
SBA-16APTES DTPA	−8.9 ± 0.7
SBA-16/HA	+2.9 ± 1.9
SBA-16/HAAPTES	+30.4 ± 1.3
SBA-16/HAAPTES DTPA	+10.3 ± 1.6

The zeta potential can change particles behavior within in vivo environments, given that the presence of electrical charges can minimize agglomeration phenomena or drive the in vitro destiny of systems.

3.5 Drug loading and in vitro release study

Ciprofloxacin is the most widely used fluoroquinolone in bone tissue bacterial infection treatment. Ciprofloxacin shows a wide spectrum of antimicrobial activity and a good penetration in many tissues, including bone tissue [27]. A high local dose can be obtained from the ciprofloxacin-loaded silica/hydroxyapatite nanocomposite. This has been used for targeted antibiotic release as a means of effectively delivering ciprofloxacin in bone with the purpose of minimizing toxicity and maximize the effectiveness of antibacterial treatment [28].

The amount of ciprofloxacin incorporated into SBA-16APTES and SBA-16/HAAPTES silica network samples was determined in the supernatant before and after the loading procedure by using UV-VIS spectroscopy, and the results are presented in Table 5. The results reveal that the SBA-16APTES sample presents similar ciprofloxacin incorporation ratio (28.5% w/w) as compared to the SBA-16/HAAPTES sample (30.6% w/w). Similar results were

Table 5 Incorporation ratio of ciprofloxacin into SBA-16APTES and SBA-16/HAAPTES

Samples	Loading ratio (%)
SBA-16APTES	28.5 ± 1.00
SBA-16/HAAPTES	30.6 ± 0.07

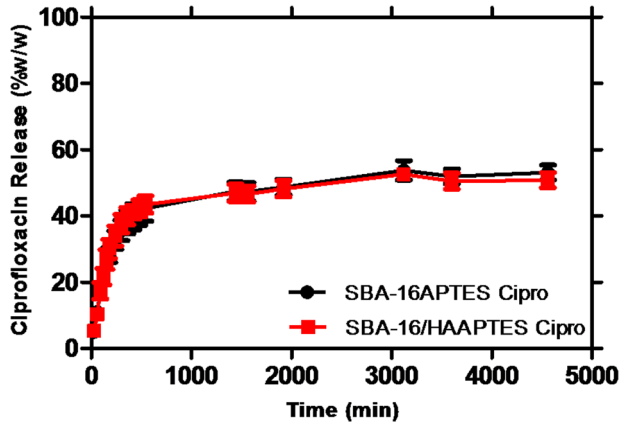

Fig. 4 Release kinetic profiles of ciprofloxacin from SBA-16APTES Cipro and SBA-16/HAAPTES Cipro samples. Values expressed as mean ± SEM

obtained by elemental analyses and TGA measurements. For SBA-16APTES Cipro sample, a ciprofloxacin incorporation percentage of 28% (w/w) was observed, and for SBA-16/HAAPTES Cipro, 31% (w/w) was obtained. This behavior might be related to the comparable surface modification with APTES in both samples.

This similar amount in the samples can be attributed to the analogous pore spaces and surface area available after functionalization for drug loading. The similar pore volume of the SBA-16APTES and SBA-16/HAAPTES can be confirmed by the nitrogen adsorption technique.

The in vitro ciprofloxacin release behavior from SBA-16APTES Cipro and SBA-16/HAAPTES Cipro samples was investigated as a function of time (Fig. 4). The release profiles of SBA-16APTES Cipro and SBA-16/HAAPTES Cipro matrices exhibited an initial burst release effect during the first 9 h, around 42% and 43% of the loading quantity released. The maximum release achieved in 76 h for the SBA-16APTES Cipro sample was approximately 53%, as compared to the SBA-16/HAAPTES Cipro samples, which reached 51%. The initial burst release can be attributed to the prompt dissolution and release of the portion of ciprofloxacin located on the surface. On the other hand, the second step exhibits a very slow and extended ciprofloxacin release which might be explained by the high affinity of the drug with amine surface group and its interactions within the inner microporous spaces [29]. According to ciprofloxacin release profiles, there was no significant difference between them.

The interaction between drug and APTES is important to understand the delivery ratio. Andrade et al. [15] have previously assessed the behavior of the system SBA-16 and SBA-16/HA without APTES during drug delivery process. Drug loading percentage inside the matrices showed a lower ratio of ciprofloxacin-incorporated than matrices functionalized with APTES. This result can be explained by the interaction of functional groups of ciprofloxacin molecule with amine groups through hydrogen bonding. These interactions could be more intense, and could explain a larger incorporation and a smaller release, when compared with interaction of ciprofloxacin with the same matrices without functionalization described by Andrade [15]. In a previous study, it was found that both surface interaction and pore volume do in fact affect the ratio and amount released from the mesoporous materials. Due to the structural characteristics of ciprofloxacin, which is a weak acid containing two pKa values, 6.09 (carboxylic acid groups) and 8.4 (nitrogen of piperazinyl ring), this is strongly influenced by pH. It is possible to perceive the strong interaction of the drug with the modified surface, both in the incorporation solution and in the release solution (SBF) at pH 7.3. In an SBF solution, the carboxylic acid was found to be dissociated, and the nitrogen of piperazinyl ring is protonated, hence it is classified as a zwitterionic species [30]. The molecule behavior can foster a greater interaction with the amine groups.

3.6 Cytotoxicity studies

To evaluate the potential of samples as an effective drug carrier for therapy, the in vitro cytotoxicity of SBA-16, SBA-16APTES, SAB-16APTES Cipro, SBA-16/HA, SBA-16/HAAPTES and SBA-16/HAAPTESCipro was investigated. In this work MTT and CellTiter assays were used in order to access cell metabolism viability [31]. MTT assay is currently considered a viability test that works efficiently in the vast majority of cases. CellTiter-Blue is a fluorescent method that indicates mitochondrial activity based on the reduction of resazurin to resorufin in metabolically active cells [32].

The percentage of MTT metabolization measured from the solubilized formazan crystals generated by viable cells is presented in Fig. 5. The reduction of resazurin to resorufin by mitochondrial activity is presented in Fig. 6. The MTT assays showed significant decrease in mitochondrial activity and cell viability in concentrations greater than 100 $\mu g\,mL^{-1}$ (Fig. 5). CellTiter analyses showed for all samples tests, no differences between lower concentration (3.2 $\mu g\,mL^{-1}$) and non-treated cells. However, higher concentrations such as 100 $\mu g\,mL^{-1}$ induced significant decrease in

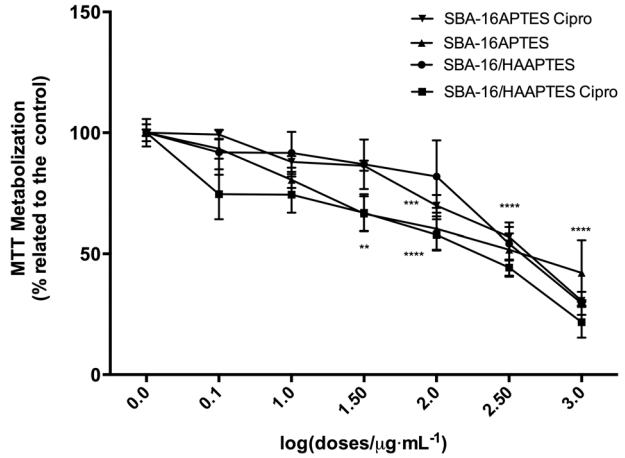

Fig. 5 Cell viability of HEK 293 incubated with different concentrations of composites using MTT reagent. 24 h after plating, cells were treated with concentrations ranging from 1.25 to 1000.0 μg/mL of SBA-16APTES, SBA-16APTES Cipro, SBA-16/HAAPTES and SBA-16/HAAPTES Cipro. The ability of cells to reduce the MTT was calculated and the materials concentrations expressed in log. The composite-treated groups were normalized related to the cell viability of control groups, non-treated cells. In high concentration of materials, there was a slight decrease in HEK 293 cell viability. Results are expressed as mean ± SEM of triplicates from three separate experiments. $^{**}p < 0.01$; $^{***}p < 0.001$; $^{****}p < 0.0001$

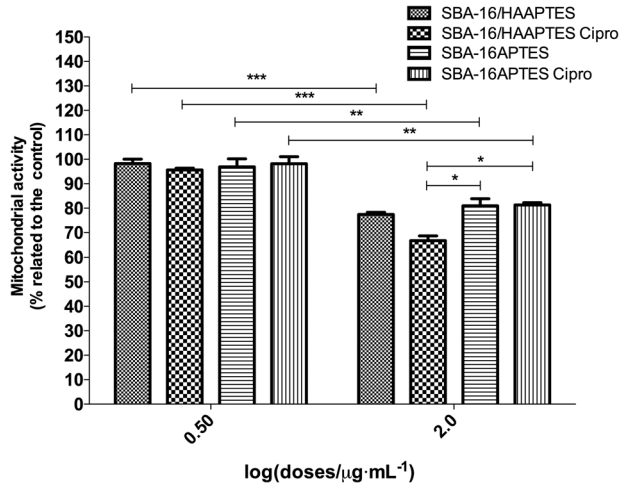

Fig. 6 HEK 293 mitochondrial activity. 1×10^4 cells/mL were plated in the presence of SBA-16, SBA-16 APTES, SBA-16APTES Cipro, SBA-16/HA SBA-16/HAAPTES and SBA-16/HAAPTES Cipro at X and Y concentrations. After 48 h, cells were incubated with CellTiter reagent for 4 h and the ability of cells to reduce the reagent were calculated. The material concentrations were expressed in log of values and the treated groups were normalized related to cell viability value presented by untreated cells (control, 100% viability). CellTiter fluorescence results showed a slight decrease in HEK 293 cell mitochondrial activity in increased amount of concentration of the materials. Results mean ± SEM of triplicates from three separate experiments. $^{*}p < 0.05$; $^{**}p < 0.01$; $^{***}p < 0.001$

mitochondrial cell metabolism. SBA-16/HAAPTES Cipro-treated cells presented a lower cell metabolism compared to SBA-16APTES and SBA-16APTES Cipro (Fig. 6). Collectively, our results showed the reduction of HEK 293 cell viability with the increase in the materials SBA-16APTES, SBA-16APTES Cipro, SBA-16/HAAPTES, SBA-16/HAAPTES Cipro concentrations.

3.7 Antimicrobial screening

The overall results of the antimicrobial assays are shown in Table 6. All samples were subjected to antimicrobial assay by broth microdilution method [23]. Gram-positive bacteria *Bacillus cereus* and *Staphylococcus aureus*, Gram-negative bacteria *Escherichia coli* and *Pseudomonas aeruginosas* were tested. Both functionalized samples containing ciprofloxacin presented a high antibacterial action against all microorganisms especially when compared to the results obtained with pure ciprofloxacin. In addition, it is important to note that the amount of free ciprofloxacin is approximately three times greater than the amount of ciprofloxacin contained in the sample. HA/SBA-16APTES Cipro has been revealed to be very active against *Staphylococcus aureus* (96.3 ± 0.8) with an inhibition value greater than ampicillin (95.9 ± 0.3) and free ciprofloxacin (76.4 ± 2.4). In the case of *Escherichia coli*, a similar behavior was observed, since the results showed a better performance of this sample (96.4 ± 0.6) in relation to free ciprofloxacin (88.3 ± 1.0) and a comparable activity in relation to ampicillin (97.5 ± 0.4). Some assays with pure samples were performed, without incorporation of the drug, to evaluate their performance in the antimicrobial process. It is important to note that samples of HA/SBA-16 and SBA-16APTES without ciprofloxacin presented moderate activity against *Escherichia coli*, with 83.4 and 77.0%, respectively. This result can indicate that the materials contribute to the antimicrobial activity [33].

3.8 Radiochemical yields

The TLC was used to predict the radiochemical yields of the ^{99m}Tc-DTPA-SBA-16APTES and ^{99m}Tc-DTPA-SBA-16/HAAPTES. The results obtained showed a mean radiochemical yield for ^{99m}Tc-DTPA-SBA-16APTES of 98.10 ± 1.02% and ^{99m}Tc-DTPA-SBA-16/HAAPTES 99.74 ± 0.08% ($n = 6$). $^{99m}TcO_4^-$ migrates to the top of the silica gel plaque when methylethylketone is used as a mobile phase (Rf = 0.9–1). On the other hand, $^{99m}TcO_2$ molecules and radiolabeled particles remain at the bottom of the silica gel plaque (Rf = 0), allowing the quantification of free technetium-99m. The presence of radiochemical impurities proved to be a drawback in nuclear medicine, yielding images with poor quality [34]. Therefore, radiochemical purity above 90% is recommended for radiopharmaceuticals, which was achieved for both ^{99m}Tc-

Table 6 In vitro growth inhibition of microorganisms induced by compounds at the concentration of 250 μg mL^{-1}

Microorganism	*Staphylococcus aureus*	*Pseudomonas aeruginosa*	*Escherichia coli*	*Bacillus cereus*
Ciprofloxacin	76.4 ± 2.4	77.4 ± 2.1	88.3 ± 1.0	85.9 ± 1.3
Ampicillin	95.9 ± 0.3	93.3 ± 0.6	97.5 ± 0.4	93.6 ± 0.7
HA/SBA-16	22.1 ± 2.0	18.0 ± 2.5	83.4 ± 0.4	9.1 ± 2.5
HA/SBA-16APTES	9.9 ± 1.5	6.0 ± 0.9	26.8 ± 3.0	9.6 ± 1.4
HA/SBA-16 APTES Cipro	96.3 ± 0.8	86.3 ± 1.8	96.4 ± 0.6	89.1 ± 1.6
SBA-16	7.2 ± 1.6	3.0 ± 0.4	25.2 ± 2.3	0
SBA-16APTES	1.6 ± 0.7	0	77.0 ± 0.5	0
SBA-16APTES Cipro	93.3 ± 0.9	88.8 ± 1.2	95.6 ± 1.5	84.6 ± 2.8

Results are mean values of quintuplicate assays ± standard deviation (expressed as % inhibition)

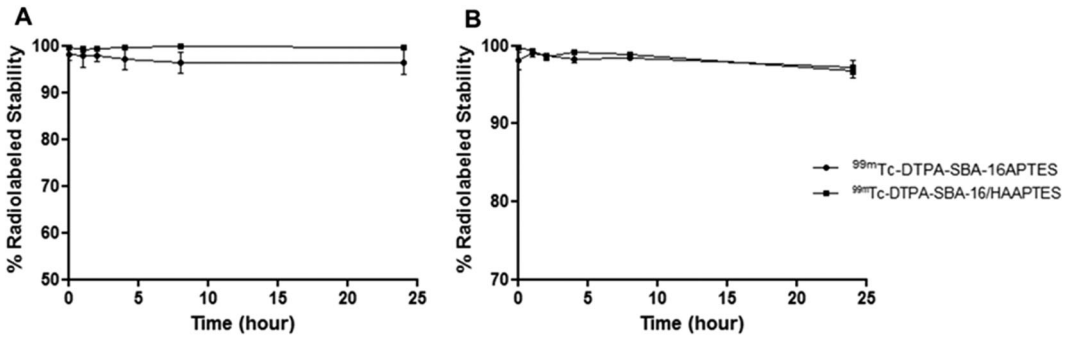

Fig. 7 In vitro stability of ^{99m}Tc-DTPA-SBA-16APTES and ^{99m}Tc-DTPA-SBA-16/HAAPTES in NaCl 0.9% (w/v) (room temperature) (**a**) and plasma (37 °C) (**b**). The data are expressed as mean ± standard deviation ($n = 3$)

DTPA-SBA-16APTES and ^{99m}Tc-DTPA-SBA-16/HAAPTES.

3.9 In vitro stability

Radiochemical stability was evaluated for the ^{99m}Tc-DTPA-SBA-16APTES and ^{99m}Tc-DTPA-SBA-16/HAAPTES at 1, 2, 4, 6, 8 and 24 h in NaCl 0.9% (w/v) solution, at room temperature, and mice plasma at 37 °C, under agitation. An excellent stability, even over long periods, was observed (Fig. 7). Radiochemical purity remained above 90% throughout all the observation period, for both complexes. In vitro stability is extremely important for radiopharmaceuticals, since particles with low radiolabeling stability will generate data that no longer reflect the nanoparticle fate.

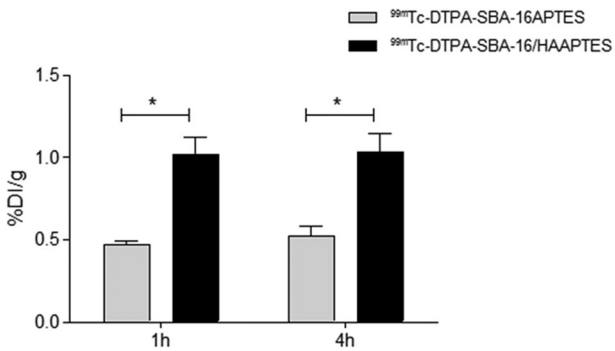

Fig. 8 Uptake of ^{99m}Tc-DTPA-SBA-16APTES and ^{99m}Tc-DTPA-SBA-16/HAAPTES by bone tissue, at 1 and 4 h post-injection. Results are expressed as mean ± SEM of triplicates from three separate experiments. * $p < 0.05$

3.10 Biodistribution studies

Results obtained from in vitro studies suggested that ^{99m}Tc-DTPA-SBA-16APTES and ^{99m}Tc-DTPA-SBA-16/HAAPTES have suitable characteristics for a radiotracer, allowing in vivo biodistribution studies, to predict the applicability of these particles [11]. As expected, both complexes were avidly uptaken by liver and spleen, and the radioactivity associated with these organs reached the highest level at 4 h post-injection. Nanostructures are normally recognized by mononuclear phagocyte system, especially by macrophages present in these organs [35]. Moreover, both radiocomplexes revealed low uptake by thyroid and stomach, which confirms in vitro stability data, since it is well known that free technetium-99m has preferential uptake by these organs [36].

Regarding to bone uptake, a higher uptake for ^{99m}Tc-DTPA-SBA-16/HAAPTES was observed when compared to ^{99m}Tc-DTPA-SBA-16APTES, at 1 and 4 h post-injection (Fig. 8). This result indicates more specificity for bone tissue for ^{99m}Tc-DTPA-SBA-16/HAAPTES. This occurs due to the presence of hydroxyapatite in the complex, which has high affinity for bone matrix [16]. Target-to-nontarget ratios confirm the affinity of these particles for bone tissue. At 4 h post-injection, this ratio was 4.34 ± 0.05 ($n = 3$), in other words, the uptake by bone tissue was 4.3 times higher than muscle tissue, used as a control group.

4 Conclusion

In this study, we have demonstrated the effective functionalization process of mesoporous silica SBA-16/Hydroxyapatite-based composite using a one-pot process by post-synthesis grafting. The applicability of these systems as a matrix for controlled drug delivery was studied and the results indicate that there was no significant difference between them. MTT and CellTiter analyses in HEK 293 cell line indicated that the presence of material in concentrations up to 100 μg mL^{-1} did not compromise the cell metabolism and consequently, cell viability. Biological activity of silica/hydroxyapatite composite with ciprofloxacin against susceptible bacteria was also evaluated and both functionalized samples containing ciprofloxacin presented a high antibacterial action against all microorganism especially when compared to the results obtained with pure ciprofloxacin. SBA-16/HA and SBA-16APTES without ciprofloxacin showed significant antimicrobial activity against *E. coli*. SBA-16/HAAPTES and SBA-16 also had antimicrobial activity, albeit in a less significant way. These results indicate that the materials have antimicrobial activity. In addition, according to biodistribution studies with radiolabel samples, the SBA-16/HAAPTES presented greater affinity than SBA-16APTES for bone tissue. Furthermore, the composite developed in this work is cost-effective and of controllable production, which indicates that our findings have significant relevance to infection bone treatment.

Acknowledgements This work was supported by funding from CAPES, CNPq, and FAPEMIG. Experiments and analyses involving electron microscopy were performed in the Microscopy Center of the Federal University of Minas Gerais, Belo Horizonte, Brazil (http://www.microscopia.ufmg.br). The authors thank the LNLS (Campinas, Brazil) for Synchrotron radiation measurements.

Compliance with ethical standards

Conflicts of interest The authors declare that they have no competing interests.

References

1. Arcos D, Vallet-Regí M (2010) Sol-gel silica-based biomaterials and bone tissue regeneration. Acta Biomater 6:2874–2888. https://doi.org/10.1016/j.actbio.2010.02.012
2. Devanand Venkatasubbu G, Ramasamy S, Ramakrishnan V, Kumar J (2011) Nanocrystalline hydroxyapatite and zinc-doped hydroxyapatite as carrier material for controlled delivery of ciprofloxacin. 3 Biotech 1:173–186. https://doi.org/10.1007/s13205-011-0021-9
3. Andersson DI, Hughes D (2010) Antibiotic resistance and its cost: is it possible to reverse resistance? Nat Rev Microbiol 8:260–271. https://doi.org/10.1038/nrmicro2319
4. Capeletti LB, Oliveira LF De, Gonçalves KDA, et al. (2014) Tailored silica-antibiotic nanoparticles: overcoming bacterial resistance with low cytotoxicity. https://doi.org/10.1021/la4046435
5. Drlica K (1999) Mechanism of fluoroquinolone action. Curr Opin Microbiol 2:504–508. https://doi.org/10.1016/S1369-5274(99)00008-9
6. Redgrave LS, Sutton SB, Webber MA, Piddock LJ (2014) Fluoroquinolone resistance: mechanisms, impact on bacteria, and role in evolutionary success. Trends Microbiol 22:438–445
7. Kim HW, Knowles JC, Kim HE (2004) Hydroxyapatite/poly (??-caprolactone) composite coatings on hydroxyapatite porous bone scaffold for drug delivery. Biomaterials 25:1279–1287. https://doi.org/10.1016/j.biomaterials.2003.07.003
8. Blasi F, Aliberti S, Tarsia P (2007) Clinical applications of azithromycin microspheres in respiratory tract infections. Int J Nanomed 2:551–559
9. Tang F, Li L, Chen D (2012) Mesoporous silica nanoparticles: synthesis, biocompatibility and drug delivery. Adv Mater 24:1504–1534. https://doi.org/10.1002/adma.201104763
10. Cassidy JW (2015) Nanotechnology in the regeneration of complex tissues. Bone Tissue Regen Insights 5:25–35. https://doi.org/10.4137/BTRI.S12331.Nanotechnology
11. Juhasz JA, Best SM (2012) Bioactive ceramics: processing, structures and properties. J Mater Sci 47:610–624. https://doi.org/10.1007/s10853-011-6063-x
12. Wu C, Chang J (2012) Mesoporous bioactive glasses: structure characteristics, drug/growth factor delivery and bone regeneration application. Interface Focus 2:292–306. https://doi.org/10.1098/rsfs.2011.0121
13. Valente FL, Reis ECC, Sepúlveda RV et al. (2016) Hydroxyapatite, polycaprolactone and alendronate composites for bone regeneration in rabbits' olecranon: histological features. Arq Bras Med Vet e Zootec 68:543–547. https://doi.org/10.1590/1678-4162-8343
14. Dasgupta S, Banerjee SS, Bandyopadhyay A, Bose S (2010) Zn- and Mg-doped hydroxyapatite nanoparticles for controlled release of protein. Langmuir 26:4958–4964. https://doi.org/10.1021/la903617e
15. Andrade GF, Gomide VS, da Silva Júnior AC et al. (2014) An in situ synthesis of mesoporous SBA-16/hydroxyapatite for ciprofloxacin release: in vitro stability and cytocompatibility studies. J Mater Sci Mater Med 25:2527–2540. https://doi.org/10.1007/s10856-014-5273-6
16. Andrade GF, Carvalho JL, Júnior ASC et al. (2015) Osteogenic differentiation of adipose-derived stem cells in mesoporous SBA-16 and SBA-16 hydroxyapatite scaffolds. RSC Adv 5:54551–54562. https://doi.org/10.1039/C5RA07330H
17. Gobin OC (2006) SBA-16 materials synthesis, diffusion and sorption properties. Laval University, Ste-Foy, Quebec, Canada

18. Díaz A, López T, Manjarrez J et al. (2006) Growth of hydroxyapatite in a biocompatible mesoporous ordered silica. Acta Biomater 2:173–179. https://doi.org/10.1016/j.actbio.2005.12.006
19. Izquierdo-Barba I, Sousa E, Doadrio JC et al. (2009) Influence of mesoporous structure type on the controlled delivery of drugs: Release of ibuprofen from MCM-48, SBA-15 and functionalized SBA-15. J Sol-Gel Sci Technol 50:421–429. https://doi.org/10.1007/s10971-009-1932-3
20. Andrade GF, Soares DCF, dos Santos RG, Sousa EMB (2013) Mesoporous silica SBA-16 nanoparticles: synthesis, physicochemical characterization, release profile, and in vitro cytocompatibility studies. Microporous Mesoporous Mater 168:102–110. https://doi.org/10.1016/j.micromeso.2012.09.034
21. de Barros ALB, de Oliveira Ferraz KS, Dantas TCS et al. (2015) Synthesis, characterization, and biodistribution studies of 99mTc-labeled SBA-16 mesoporous silica nanoparticles. Mater Sci Eng C 56:181–188. https://doi.org/10.1016/j.msec.2015.06.030
22. Ehlert N, Badar M, Christel A et al. (2011) Mesoporous silica coatings for controlled release of the antibiotic ciprofloxacin from implants. J Mater Chem 21:752. https://doi.org/10.1039/c0jm01487g
23. Cueva C, Moreno-Arribas MV, Martín-Álvarez PJ et al. (2010) Antimicrobial activity of phenolic acids against commensal, probiotic and pathogenic bacteria. Res Microbiol 161:372–382. https://doi.org/10.1016/j.resmic.2010.04.006
24. Beck JS, Vartuli JC, Roth WJ, et al. (1992) A new family of mesoporous molecular sieves prepared with liquid crystal templates. J Am Chem Soc 10834. https://doi.org/10.1021/ja00053a020
25. Costa JAS, Garcia ACFS, Santos DO et al. (2014) A new functionalized MCM-41 mesoporous material for use in environmental applications. J Braz Chem Soc 25:197–207. https://doi.org/10.5935/0103-5053.20130284
26. Pang J, Zhao L, Zhang L et al. (2013) Folate-conjugated hybrid SBA-15 particles for targeted anticancer drug delivery. J Colloid Interface Sci 395:31–39. https://doi.org/10.1016/j.jcis.2012.12.016
27. Mouriño V, Boccaccini AR (2010) Bone tissue engineering therapeutics: controlled drug delivery in three-dimensional scaffolds. J R Soc Interface 7:209–227. https://doi.org/10.1098/rsif.2009.0379
28. Gao P, Nie X, Zou M et al. (2011) Recent advances in materials for extended-release antibiotic delivery system. J Antibiot64:625–634. https://doi.org/10.1038/ja.2011.58
29. Moritz M, Geszke-Moritz M (2015) Mesoporous materials as multifunctional tools in biosciences: principles and applications. Mater Sci Eng C Mater Biol Appl 49:114–151. https://doi.org/10.1016/j.msec.2014.12.079
30. Babić S, Horvat AJM, Mutavdžić Pavlović D, Kaštelan-Macan M (2007) Determination of pKa values of active pharmaceutical ingredients. TrAC Trends Anal Chem 26:1043–1061. https://doi.org/10.1016/j.trac.2007.09.004
31. Berridge MV, Herst PM, Tan AS (2005) Tetrazolium dyes as tools in cell biology: new insights into their cellular reduction. Biotechnol Annu Rev 11:127–152. https://doi.org/10.1016/S1387-2656(05)11004-7
32. Bancos S, Tsai D-H, Hackley V et al. (2012) Evaluation of viability and proliferation profiles on macrophages treated with silica nanoparticles in vitro via plate-based, flow cytometry, and coulter counter assays. ISRN Nanotechnol 2012:1–11. https://doi.org/10.5402/2012/454072
33. Pereira VV, Silva RR, Duarte LP, Takahashi JA (2016) Chemical constituents of Jacaranda oxyphylla and their acetylcholinesterase inhibitory and antimicrobial activities. Rec Nat Prod 10:392–396
34. de Barros ALB, Mota L das G, Ferreira C de A, Cardoso VN (2012) Kit formulation for 99mTc-labeling of HYNIC-BAla-Bombesin (7–14). Appl Radiat Isot 70:2440–2445. https://doi.org/10.1016/j.apradiso.2012.06.022
35. Shin SJ, Beech JR, Kelly KA (2012) Targeted nanoparticles in imaging: paving the way for personalized medicine in the battle against cancer. Integr Biol 5:29–42. https://doi.org/10.1039/c2ib20047c
36. James H, Thrall HAZ (2003) Medicina Nuclear. In: G Koogan (ed) 2a edn. p. 408. ISBN 852770790X